Study of a 5 T Research Dipole Insert-Magnet using an Anisotropic ReBCO Roebel Cable

J. van Nugteren, G.A. Kirby, G. de Rijk, L. Rossi, H.H.J. ten Kate
CERN, Geneva, Switzerland

M.M.J. Dhallé
University of Twente, Drienerlolaan 5, Enschede, Netherlands.

Abstract

A design study is presented for the coil layout of theEUCARD-2 Five Tesla HTS Research (FeaTHeR) magnet. The angular dependence of the critical current in the used ReBCO Roebel cable is taken into account. This leads to a new coil layout named aligned block. This layout makes optimal use of the anisotropy of the ReBCO coated conductor, by aligning all tapes with the magnetic field lines. Both two dimensional cross sections and three dimensional coil layouts are presented. In the layouts the magnetic field angle is highest at the edges of the cable causing a large variation of the critical current over its width. Different approaches to the calculation of the critical current, with and without current sharing in and between the tapes, are presented. The values are compared to the values found using a non-linear network model of the cable, in which the electrical properties of the elements are calculated as a function of magnetic field and magnetic field angle. The model also includes electrical contact between the strands using additional network elements.

Presented at: ASC 2014, 10-15 August, Charlotte, USA

Geneva, Switzerland
June 2015

Study of a 5 T Research Dipole Insert-Magnet using an Anisotropic ReBCO Roebel Cable

J. van Nugteren, G.A. Kirby, G. de Rijk, L. Rossi, H.H.J. ten Kate (CERN) and M.M.J. Dhallé (Twente)

Abstract—A design study is presented for the coil layout of the EUCARD-2 Five Tesla HTS Research (FeaTHeR) magnet. The angular dependence of the critical current in the used ReBCO Roebel cable is taken into account. This leads to a new coil layout named aligned block. This layout makes optimal use of the anisotropy of the ReBCO coated conductor, by aligning all tapes with the magnetic field lines. Both two dimensional cross sections and three dimensional coil layouts are presented. In the layouts the magnetic field angle is highest at the edges of the cable causing a large variation of the critical current over its width. Different approaches to the calculation of the critical current, with and without current sharing in and between the tapes, are presented. The values are compared to the values found using a non-linear network model of the cable, in which the electrical properties of the elements are calculated as a function of magnetic field and magnetic field angle. The model also includes electrical contact between the strands using additional network elements.

Index Terms—HTS, ReBCO, YBCO, Roebel cable, accelerator magnet, aligned Block

I. INTRODUCTION

As part of the Future Circular Collider (FCC) hadron-hadron collider study [1], a new domain of high-field dipole magnets is required. At present there are two different target fields, $16\,\text{T}$ and $20\,\text{T}$. The first lies at the limit of the Nb_3Sn conductor. The second will require the use of High Temperature Superconductors (HTS) at the inner, high-field, part of the hybrid magnet [2], [3]. The first steps towards these HTS insert-magnets have already been made over the last years, within work-package 7 of the EuCARD-1 collaboration [4]. These efforts will be continued in EuCARD-2, resulting in a useful synergy with the FCC study. Work-package 10.3 of EuCARD-2 concerns the design and construction of a Five Tesla High Temperature Superconductor (HTS) Research (FeaTHeR) magnet [5], [6], [7]. This magnet is required to generate a $5\,\text{T}$ central operating field in a $40\,\text{mm}$ aperture (with a reasonable field quality). To achieve a low magnet inductance and to allow, in future perspective, possible series operation with $\text{Nb-Ti}/\text{Nb}_3\text{Sn}$ coils, a $10\,\text{kA}$ class cable is required. By restricting the outer diameter of the magnet to $99\,\text{mm}$ (this leaves $1\,\text{mm}$ margin for adding extra insulation sheets) and by adding additional mechanical structure, it can be tested as an insert inside the Fresca-2 magnet [8].

In this paper the focus is on an *aligned block* layout option for the ReBCO coated conductor EuCARD-2 magnet. The critical current of the coated conductor tapes is highly anisotropic (see Fig. 1), which means that it strongly depends on the angle of the magnetic field with respect to the surface of the conductor. This anisotropy becomes more pronounced in high magnetic fields, at which the difference in critical current, between the good parallel and bad perpendicular magnetic field, can be as much as a factor five. In this novel layout the magnetic field angle with respect to the orientation of the conductor is minimized. This magnet is named Feather-M2. An initial development step, to test coil winding and quench protection, in the form of a smaller single racetrack coil named Feather-M0 is foreseen. This racetrack coil can be tested standalone in an iron yoke or in the existing Fresca facility [9].
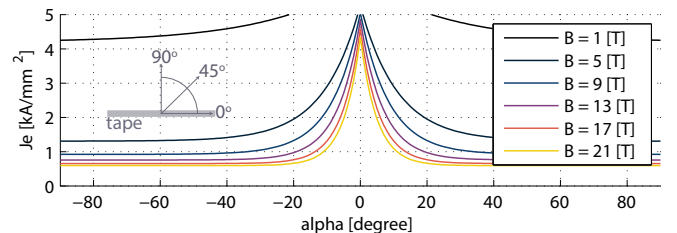

Fig. 1. The engineering current density that is used for the ReBCO superconducting tape as function of the magnetic field angle and magnitude. The fit is based on measurement data on SuperPower tapes performed by NHFML [10] and is scaled with a factor 1.5 to the EuCARD-2 engineering current density requirement of $600\,\text{A}/\text{mm}^2$ over the tape at $20\,\text{T}$ perpendicular applied magnetic field.

Both designs are based on the Roebel cable because it meets the current density requirement, is fully transposed and all tapes are oriented in the same direction [11]. The geometry and parameter values of the cable are provided in Fig. 2 and Table I, respectively. Due to the self-field in the aligned block design the edges of the cable still see the magnetic field under a small angle. This leads to a strong variation of the critical current across the width of the strands and cable. Because the wide tapes behave as large mono-filaments, the superconducting current can flow freely from one side of the tape to the other. Different methods of calculating the critical current are presented. The results of these methods are compared to an electrical network model representing the Roebel cable in the coil.

II. CROSS SECTIONAL LAYOUT

The Feather-M2 magnet is designed to operate in two different scenarios. The first is standalone operation inside
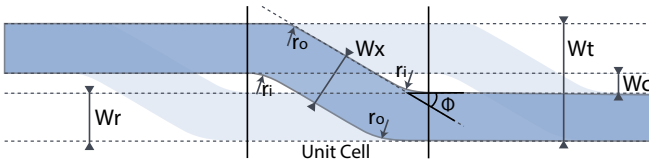
Fig. 2.   Definition of parameters for the geometry of a Roebel cable [12].

TABLE I
PARAMETER VALUES OF THE COATED CONDUCTOR AND ROEBEL CABLE.

| Symbol	FM0	FM2	Description
Ns	15	15	number of strands
ds	0.10 mm	0.10 mm	strand thickness
dc	0.8 mm	0.8 mm	cable total thickness
di	0.1 mm	0.1 mm	insulation thickness
Wr	5.50 mm	5.50 mm	strand width
Wt	12.0 mm	12.0 mm	cable width
Wx	5.50 mm	5.50 mm	cross over width
Wc	1.0 mm	1.0 mm	channel width
Φ	30 degree	30 degree	cross over angle
Ltp	226 mm	226 mm	transposition pitch
ri	6.0 mm	6.0 mm	inner radius
ro	0.0 mm	0.0 mm	outer radius
$fimp$	1.0	1.5	improvement factor
$J_{20T\perp}$	400 A/mm^2	600 A/mm^2	tape Je at 20 T $\perp$
$Abare$	9.6 mm^2	9.6 mm^2	bare cable area
$Ainsu$	12.2 mm^2	12.2 mm^2	total cable area
$fvoid$	~ 0.10	~ 0.10	void factor
$finsu$	~ 0.20	~ 0.20	insulation factor

Fig. 3.   Two dimensional coil layout showing one pole and axial projection of the flared-end. On the left shown for the wing deck and on the right for the central deck.
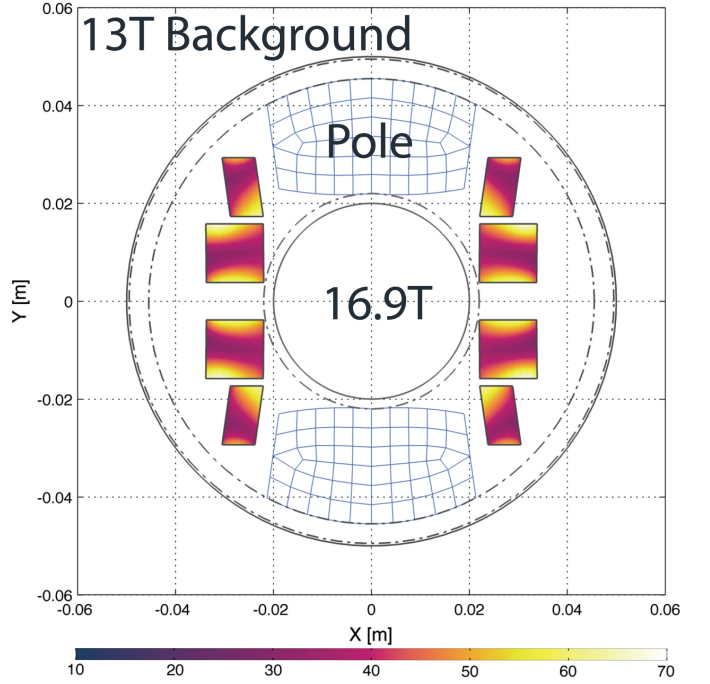

Fig. 4.   Percentage on the load-line plotted in a cross section of the Feather-M2 when operated in a background field of 13 T.

an iron yoke generating 5 T with reasonable geometric field quality ($b_3 = 0$) at a reference radius of 13.33 mm. The second is in a 13 T background field, generating as much magnetic field as possible, without imposing any field quality requirements [13]. To maximize the magnetic field in the second scenario, the off-vertical angle of the blocks is adjusted to align the conductor orientation with the magnetic field lines in the background field. At the same time the harmonics and the width of the coil blocks are optimized for the standalone case. The resulting layout of the Feather-M2 and a projection of the blocks towards the coil ends is presented in Fig. 3. To keep the windings within the support cylinder, the width of the coil blocks is limited by the volume available at the coil ends. An iron pole piece is added to help align the magnetic field and to provide an extra 0.4 T at the center of the aperture. The coil is designed to reach 5 T when operating at 70% on the load-line. The unusual position of the short sample compared to classical magnets is presented in Fig. 4. A target conductor performance of 600 A/mm^2 in the tape at 20 T perpendicular applied field is assumed. Due to the alignment the calculated operating current is almost equal in standalone and in the background field. The difference in magnetic field contribution is mainly caused by the absence of the iron yoke, reducing the field to a total of 16.9 T. However, the relatively high current density may make the quench protection of the magnet more difficult [14]. This will be verified experimentally using Feather-M0.

III. THREE DIMENSIONAL LAYOUT

To achieve proper alignment in three dimensions is challenging. The coil geometry of Feather-M2 and the definition of
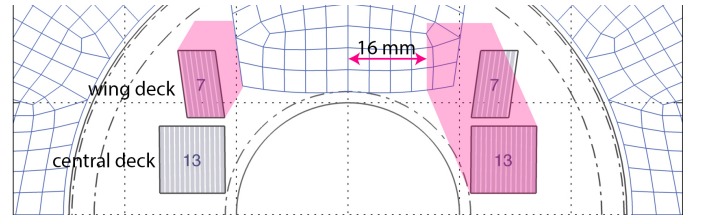
the parameters is shown in Fig. 5. The values of the parameters used for Feather-M0 and Feather-M2 are presented in Table II. The side view defines the flaring of the end and is mainly determined by the hard-way bend radius of the cable, which is determined experimentally using a dummy cable. The angle at which the flared end deviates from the mid-plane of the magnet, determines the off-vertical angle at the end of the coil and is set to 4 degree (this also determines the average field angle there). The coil can be divided in three sections: a straight section, a curved section and a sloped section. Note that in this coil the straight section is only around 100 mm long. The plan view is mainly determined by the easy-way bend radius of the cable and the restriction on the outer radius of the coil. The bend radius at the coil end of the central deck is set at 16 mm, which is at a safe margin from the easy-way limit of 11 mm [15]. This then leads to the typical diamond shape (rhombus). The wing deck and central deck are nested to allow for a layer jump to connect the two. The length of the wing deck is shorter than the central deck to prevent it from hitting the support cylinder. Additional iron pole pieces are added inside the coil ends to help straighten the field. Because the blocks move away from the mid-plane towards
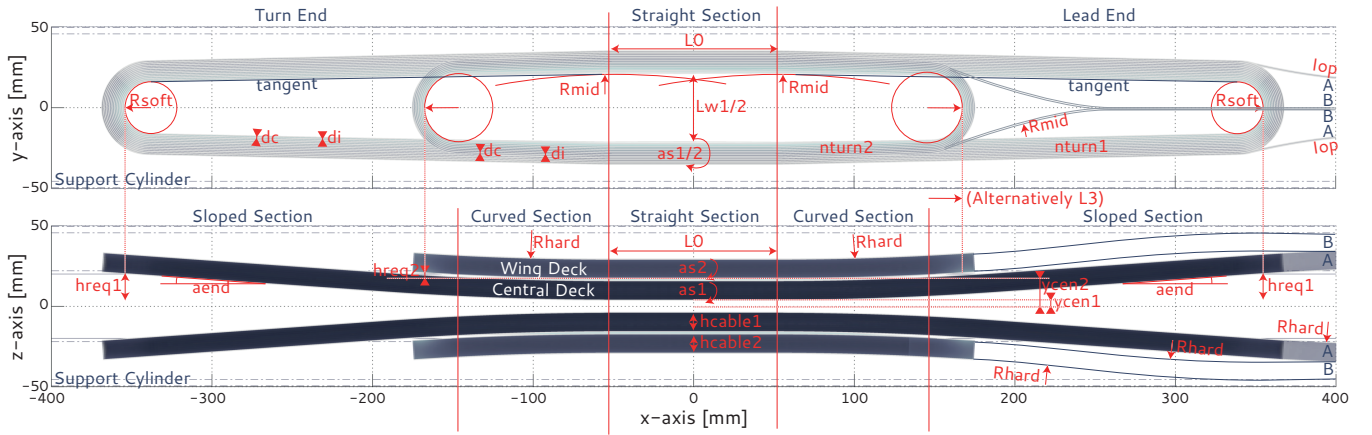
Fig. 5. Definition of parameters for the Feather-M0 and Feather-M2 coil layouts presented using top and side projections of the three dimensional coil layout.

TABLE II
GEOMETRIC SPECIFICATIONS OF THE THREE-DIMENSIONAL COIL
LAYOUTS OF FEATHER-M0 AND FEATHER-M2.

Symbol	FM0	FM2	Description
$mirror$	none	anti	mirror feature
ϕ_{in}	40.0 mm	40.0 mm	aperture diameter
ϕ_{out}	99.0 mm	99.0 mm	outer diameter
$drap$	n.a.	2.0 mm	extra aperture spacing
$Ryoke1$	36.0 mm	51.0 mm	yoke inner radius
$Ryoke2$	80.0 mm	111.0 mm	yoke outer radius
$Lyoke$	280.0 mm	800.0 mm	yoke length
$nturn1$	5	2×13	central deck # turns
$nturn2$	n.a.	2×7	wing deck # turns
$L0$	40.0 mm	100.0 mm	straight section length
$L3$	440.0 mm	n.a.	enforced coil length
Lw	40.0 mm	44.0 mm	straight section width
Lco	440 mm	720 mm	total coil length
Lca	5 m	2×26 m	cable length
$ycen1$	−6.0 mm	3.8 mm	central deck y-position
$ycen2$	n.a.	17.3 mm	wing deck y-position
$hreq1$	0.0 mm	17.5 mm	central deck flaring
$hreq2$	n.a.	4.0 mm	wing deck flaring
$aend$	0.0 degree	4.0 degree	angle at end
$as1$	0.0 degree	0.5 degree	central shear angle
$as2$	n.a.	8.0 degree	wing shear angle
$ptwist$	n.a.	0.6	shear angle factor
$Reasy$	16.0 mm	16.0 mm	easy-way bend radius
$Rmid$	400 mm	400 mm	mid-coil bend radius
$Rhard$	2000 mm	2000 mm	hard-way bend radius
Lco	10 μH	0.45 mH	coil self-inductance
$Mfr2$	n.a.	1.32 mH	mutual-inductance

TABLE III
OPERATIONAL SPECIFICATIONS FOR FEATHER-M0 AND FEATHER-M2
WHEN OPERATED STANDALONE INSIDE AN IRON YOKE AT 4.2 K.

Symbol	FM0	FM2	Description
$Bcen$	1.5 T	5.0 T	operating field
P_{coil}	4 MPa	17 MPa	coil pressure
Iop	6.0 kA	7.92 kA	cable operating current
J_{block}	491 A/mm^2	649 A/mm^2	block op. cur. density*
J_{cable}	625 A/mm^2	824 A/mm^2	cable op. cur. density*
Ic_{I}	11.3 kA	10.3 kA	first short sample†
Ic_{II}	14.0 kA	11.8 kA	second short sample†
Ic_{III}	16.1 kA	14.2 kA	third short sample†
Ic_{el}	13.8 kA	11.7 kA	electrical model s.s.†

TABLE IV
OPERATIONAL SPECIFICATIONS FOR FEATHER-M0 AND FEATHER-M2
WHEN OPERATED INSIDE A 13 T BACKGROUND FIELD AT 4.2 K.

Symbol	FM0	FM2	Description
outsert	Fresca	Fresca-2	outsert magnet
Bbg	8.5 T	13.0 T	background field
$Bcen$	9.2 T	16.9 T	field in aperture
P_{coil}	23 MPa	110 MPa	average coil pressure
Iop	6.0 kA	8.14 kA	cable operating current
J_{block}	491 A/mm^2	667 A/mm^2	block op. cur. density*
J_{cable}	625 A/mm^2	847 A/mm^2	cable op. cur. density*
Ic_{I}	10.6 kA	8.5 kA	first short sample†
Ic_{II}	13.2 kA	11.6 kA	second short sample†
Ic_{III}	14.9 kA	13.9 kA	third short sample†
Ic_{el}	11.8 kA	12.0 kA	electrical model s.s.†

∗ the difference in block and cable current density is the insulation area
† see Section IV and V for expanded explanation

the coil ends, the influence of the other pole on the magnetic field becomes less apparent, allowing the blocks to rotate back to vertical such that a standard racetrack coil end can be made. This local rotation of the cable is calculated from the vertical position of the coil block along the length of the magnet ($y(x)$) using

$$arot(x) = as \left[1 - \frac{y(x) - ycen}{hreq} \right]^{ptwist}, \qquad (1)$$

where $arot$ is the local rotation of the conductor (see Fig. 6), as and $ycen$ are the rotation and vertical position of the conductor at the center of the magnet, and $hreq$ the vertical displacement of the coil end. The magnetic field is calculated using a code named Field 2014 [16], which is based on a Biot-Savart Multi-Level Fast Multipole Method (MLFMM) [17].

The three-dimensional geometry and the incident angle of the magnetic field, when operated at design current in a background field of 13 T, is presented in Fig 7. It can be seen that the largest angle of 14 degree is located at edge of the cable in the coil ends. At each position along the cable there is a point where the magnetic field angle is zero. The field angle averaged over the width of the cable is always less than 4 degree.

IV. CRITICAL CURRENT CALCULATION

Due to the angle dependence of the conductor and the current redistribution inside the tapes, the calculation of the critical current is not straight forward. For a more detailed study, a model of the Roebel cable is used. The full geometry
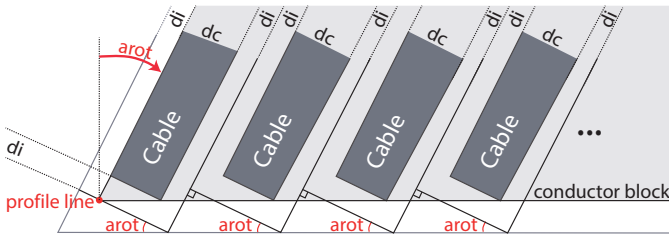
Fig. 6. Cross section of the coil block showing the definition of the rotation angle and the placement of the cables.
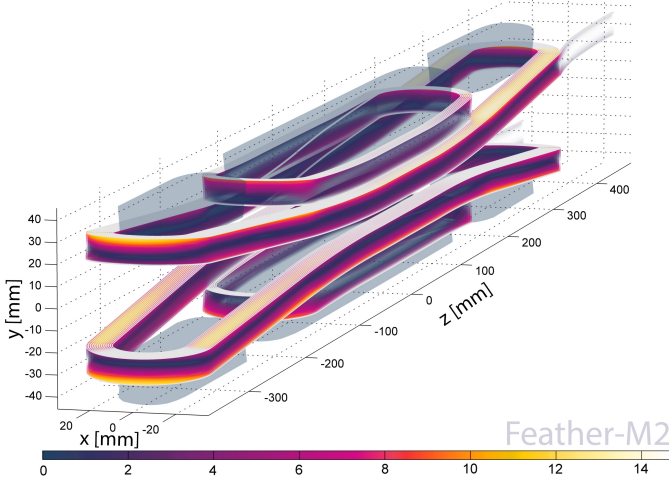

Fig. 7. Three dimensional coil layout and incident angle of the magnetic field plotted on the conductor for the Feather-M2 when operated in a background field of $13\,\mathrm{T}$.
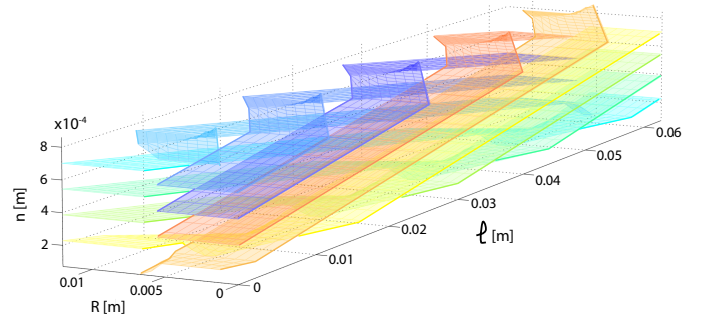

Fig. 8. Expanded view of a KIT Roebel cable showing the transposed trajectories of the tapes. Note that the vertical direction has been scaled by a factor of 10 for viewing purposes.
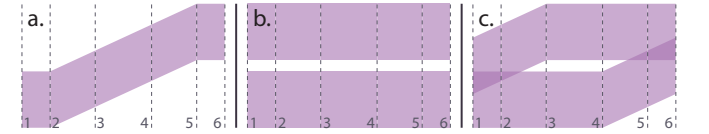

Fig. 9. Tape sections making up the geometry of the Roebel cable: the cross over bridge when located at the center of the unit cell (a); the sloped tapes (b) and the cross over bridge at the edge of the unit cell (c).

of the Roebel cable (as shown in Fig. 8) can be represented by a unit cell (with length L_{tp}/Ns). The unit cell contains a cross over strand named bridge on either side of the cable. The structure of the unit cell can be represented by a total of three different basic shapes (see Fig. 9). Using a coordinate transformation the geometry of the cable is mapped onto the coils. Multiple methods for calculating the critical current are proposed. The specifications of the two magnets including the calculated values for the critical current are given in Table III and Table IV. The first Ic_{I} conservatively assumes that no current sharing can occur and that the current is limited by the lowest Jc anywhere in the coil. The second critical current Ic_{II} assumes that current re-distribution can occur within the strand but not between the strands. This is a logical assumption since the tapes, unless striated, are fully superconducting. The calculation integrates the critical current of each tape in the cable over its width and then takes the lowest value found along the length. The lowest values of all tapes are added to find the short sample current of the cable. The third critical current Ic_{III} assumes full current sharing in and between the tapes. This can only occur if the contact resistance between the strands is very low and is therefore likely an overestimate. It is calculated by integrating the critical current density over the width of the cable, after which the lowest value is selected.

V. ELECTRICAL NETWORK MODEL

The critical current can also be calculated using the steady state solution of an electrical PEEC [18] network representing the surface of tapes using a grid of superconducting elements. Between the tapes additional contact elements, with electrical resistance $0.29\,\mu\Omega\mathrm{m}^2$ [19], are added. The electrical currents inside all elements and the voltages at the nodes are calculated by solving Kirchhoff's laws. The nature of the superconducting elements in the system causes the equations to become highly non-linear. A steady state and since recently also transient behavior can be studied using the Sundials KinSol and IDA solvers, respectively [20], resulting in a similar solver setup as the JackPot-AC model for Cable-In-Conduit Conductors [21]. The magnetic field contribution of the iron poles is calculated using a BEM-FEM algorithm [22] to create a set of field maps, which when solving are then interpolated at the cable current. For this the critical current is derived from the calculated EI-curve of the coil, using a power law fit. The electric field criterion is taken at $10\,\mu\mathrm{V/m}$.

VI. CONCLUSION

A new and optimized layout for ReBCO coated conductor dipole coils, named *aligned block*, was introduced. This layout takes advantage of the anisotropy of the conductor, by optimizing the alignment of the tapes with respect to the magnetic field lines. The design, although in its initial phase, addresses most issues related to the use of Roebel cable for a dipole magnet. Because current can flow freely in the tapes from side to side the calculation of the critical current is not straight forward. Different methods for the calculation of the critical current are introduced and compared to results following a steady state PEEC network model. The values found from the second method, which assumes current sharing within the strands, lie closest to the critical current from the network model. As a next step it is planned to use the network geometry and solver setup to model dynamic effects inside the cable or coil such as normal zone propagation.

References

[1] "Future circular colider study," available from: https://espace2013.cern.ch/fcc/Pages/default.aspx.

[2] P. McIntyre and A. Sattarov, "On the Feasibility of a Tripler Upgrade for LHC," in *Proceedings of 2005 Particle Accelerator Conference, Knoxville, Tennessee*.   IEEE, 2005, pp. 634–636.

[3] L. Rossi and E. Todesco, "Conceptual design of 20 T dipoles for high-energy LHC," in *The High-Energy Large Hadron Collider*, E. Todesco and F. Zimmermann, Eds.   CERN, April 2011, pp. 13–19.

[4] G. de Rijk, "The EuCARD High Field Magnet Project," *IEEE Transactions on Applied Superconductivity*, vol. 22, no. 3, June 2012.

[5] L. Rossi *et al.*, "The EuCARD-2 Future Magnets project: the European collaboration for accelerator quality HTS magnets," in *Applied Superconductivity Conference Proceedings*.   IEEE Transactions on Applied Superconductivity, August 2014, this conference.

[6] G. Kirby, J. van Nugteren, G. de Rijk *et al.*, "Accelerator quality HTS dipole magnet demonstrator designs for the EuCARD2, 5 T 40 mm clear aperture magnet," in *Applied Superconductivity Conference Proceedings*. IEEE Transactions on Applied Superconductivity, August 2014, this conference.

[7] C. Lorin, M. Durante, P. Fazilleau *et al.*, "Cos-theta design of dipole inserts made of YBCO-Roebel or BiSCCo-Rutherford cables," in *Applied Superconductivity Conference Proceedings*.   IEEE Transactions on Applied Superconductivity, August 2014, this conference.

[8] P. Ferracin, M. Devaux, M. Durante *et al.*, "Development of the EuCARD Nb_3Sn dipole magnet FRESCA2," in *Apllied Superconductivity Conference Proceedings*, vol. 23.   IEEE Transactions on Applied Superconductivity, June 2013.

[9] A. Verweij, J. Genest, A. Knezovic *et al.*, "1.9 K test facility for the reception of the superconducting cables for the LHC ," *IEEE Transactions on Applied Superconductivity*, vol. 9, no. 2, pp. 153 – 156, June 1999.

[10] A. Xu, J. J. Jaroszynski, F. Kametani *et al.*, "Angular dependence of jc for ybco coated conductors at low temperature and very high magnetic fields," *Superconductor Science and Technology*, vol. 23, 2010.

[11] J. Fleiter, A. Ballarino, W. Goldacker, and A. Kario, "Characterization of Roebel cables for potential use in high-field magnets," in *Applied Superconductivity Conference Proceedings*.   IEEE Transactions on Applied Superconductivity, August 2014, this conference.

[12] V. Lombardo, E. Barzi, D. Turrioni *et al.*, "Fabrication, qualification and test of high Jc Roebel $YBa_2Cu_3O_{7-\delta}$ coated conductor cable for HEP magnets," *IEEE Transactions on Applied Superconductivity*, vol. 21, pp. 2331–2334, 2011.

[13] J. van Nugteren, "Case Study for a Five Tesla HTS Research-Magnet," CERN, Tech. Rep. EDMS-1389718, June 2014.

[14] E. Härö *et al.*, "Quench considerations and protection scheme of a high field HTS dipole insert coil," *IEEE Transactions on Applied Superconductivity*, vol. 23, 2013.

[15] W. Goldacker, A. Frank, R. Heller *et al.*, "ROEBEL Assembled Coated Conductors (RACC): Preparation, Properties and Progress," *IEEE Transactions on Applied Superconductivity*, vol. 17, no. 2, pp. 3398–3401, June 2007.

[16] J. Nugteren van, "Internship Report: CERN, Software development for the Science and Design behind Superconducting Magnet Systems," Twente University: Energy Materials and Systems and CERN: ATLAS magnet team, Tech. Rep., 2011.

[17] L. Greengard and V. Rokhlin, "A fast algorithm for particle simulations," *Journal of Computational Physics*, pp. 325–348, 1987.

[18] A. Ruehli, "Equivalent Circuit Models for Three-Dimensional Multiconductor Systems," *IEEE Transactions on Microwave Theory and Techniques*, vol. 22, no. 3, 1974.

[19] K. Yagotintsev, P. Gao, M. Dhalle *et al.*, "AC loss tests on CORC and stacked tape ReBCO cables," Poster presented at ASC 2014, August 2014, charlotte (SC) USA.

[20] A. Hindmarsh, P. Brown, K. Grant *et al.*, "SUNDIALS: Suite of Nonlinear and Differential/Algebraic Equation Solvers," *ACM Transactions on Mathematical Software*, vol. 31, no. 3, pp. 363–396, September 2005.

[21] E. P. A. Van Lanen and A. Nijhuis, "Simulation of interstrand coupling loss in cable-in-conduit conductors with JackPot-AC," *IEEE Transactions on Applied Superconductivity*, vol. 21, no. 3 PART 2, pp. 1926–1929, 2011.

[22] S. Russenschuck, *Field Computation for Accelerator Magnets*.   Wiley, 2010.